PNAS

Supporting Information for

MipZ caps the plus-end of FtsZ polymers to promote their rapid disassembly

Laura Corrales-Guerrero, Wieland Steinchen, Beatrice Ramm, Jonas Mücksch, Julia Rosum, Yacine Refes, Thomas Heimerl, Gert Bange, Petra Schwille, Martin Thanbichler

Laura Corrales-Guerrero, Martin Thanbichler
Email: laucorge@us.es, thanbichler@uni-marburg.de

This PDF file includes:

Supporting Information Text
Figures S1 to S10
Tables S1 to S3
Legends for Datasets S1 to S4
SI References

Other supporting materials for this manuscript include the following:

Dataset S1
Dataset S2
Dataset S3
Dataset S4

Supporting Information Text

Extended Materials and Methods

Media and growth conditions

C. crescentus CB15N and its derivatives were cultivated at 28 °C in PYE medium (0.2% peptone, 0.1% yeast extract, 1 mM $MgSO_4$, 0.5 mM $CaCl_2$), supplemented with antibiotics when appropriate at the following concentrations (μg ml^{-1}; liquid/solid medium): kanamycin (5/25), streptomycin (5/5), spectinomycin (25/50). To induce the expression of genes placed under the control of the Pxyl (1) or Pvan (2) promoters, media were supplemented with 0.3% (w/v) D-xylose or 0.5 mM sodium vanillate.

E. coli TOP10 (Invitrogen, USA) or Rosetta(DE3)pLysS (Novagen, Germany) were used for general cloning purposes or protein overproduction. *E. coli* cells were cultivated aerobically at 37 °C in Luria-Bertani (LB) broth, supplemented with the following antibiotics if appropriate (μg ml^{-1}; liquid /solid medium): ampicillin (200/200) or chloramphenicol (20/30). When required, glucose was added to a concentration of 1% (w/v). Protein overproduction was induced by addition of 1 mM isopropyl-β-thiogalactopyranoside (IPTG).

Plasmid and strain construction

The oligonucleotides, plasmids and bacterial strains used in this work are listed in Tables S1-S3. All newly constructed plasmids were verified by DNA sequencing. Proper chromosomal integration or gene replacement were verified by colony PCR.

To generate pLT7 and pLT11, plasmid pMT183 was subjected to site-directed mutagenesis by inverse PCR (QuickChange II Site-Directed Mutagenesis Kit, Agilent Technologies, USA) with the mutagenic primer pairs MipZ-R167AK168A-for/-rev and MipZ-K208AR209A-for/-rev, respectively. To generate pLC45, plasmid pLT7 was subjected to inverse PCR with the mutagenic primer pair MipZ-K155A-for/-rev. To construct pLC46, plasmid pMT183 was subjected to two rounds of inverse PCR using primer pairs MipZ-R194A-for/-rev and MipZ-R219A-for/-rev, respectively. To obtain plasmids pLC50 and pLC51, the *mipZF3* and *mipZD2* alleles were PCR-amplified from pLC45 and pLC46, respectively, using the primer pair MipZ-Gib-for/-rev. The resulting fragments were then joined with the backbone of *Nde*I/*Sac*I-treated plasmid pBH78 by Gibson assembly (3). Plasmid pJR99 was generated by fusion of *Xba*I/*Sac*I-treated pTB146 with with a synthetic DNA fragment that contained the coding sequence for the StrepII tag and a short linker (WSHPQFEKGSGS) followed by an *Nde*I restriction site. It enables the overproduction of His_6-SUMO-StrepII tag fusions that are cleaved into the His_6-SUMO tag and a StrepII (WSHPQFEKGSGSHM)-tagged protein of interest after Ubi1 treatment (4). To construct pJR104, a fragment containing full-length *ftsZ* was PCR-amplified with primer pairs Gibson_Strep_ftsZ_for/Gibson_ftsZ_rev and fused with *Nde*I/*Sac*I-treated pJR99 by Gibson assembly. To generate pJR105, a fragment of *ftsZ* encoding a truncated protein lacking the the N-terminal disordered region and the NTD ($FtsZ_{\Delta N}$) was PCR-amplified with primer pair FtsZC_NdeI/ FtsZ_full_SacI, cut with *Nde*I and *Sac*I and ligated with *Nde*I/*Sac*I-treated pJR99. Plasmid pJR106 was generated by fusion of *Nde*I/*Sac*I-treated pJR99 with a synthetic DNA fragment encoding the a truncated FtsZ variant that only comprises helix H7 and the CTD ($FtsZ_{\Delta NC}$). To generate plasmids pJR100-pJR103, pMT183 was subjected to site-directed mutagenesis using primer pairs MipZ-L161A-for/-rev, MipZ-W164A-for/-rev, MipZ-K168A-for/-rev or MipZ-L172A-for/-rev, respectively. Plasmids pJR107-pJR111 were constructed by amplification of the *mipZ* allele from plasmids pJR100, pJR101, pJR102, pJR103 or pLT11, respectively, with primer pair MipZ-uni2/MipZ-rev10, restriction with *Nde*I and *Sac*I, and insertion of the fragment into pXYFPC-2 cut with the same enzymes. To generate pBH100, a fragment containing *mipZ* was PCR-amplified with primer pair MipZ-uni2/MipZ-rev-EcoRI, treated with *Nde*I and *Eco*RI, and ligated into the *Nde*I/*Eco*RI-treated vector pVCERN-1.

For the construction of pTR11, pTR32, pTR33 and pTR34, the *mipZ*, $mipZ_{K13A}$, $mipZ_{K18Q}$ and $mipZ_{G14V}$ alleles were PCR-amplified from plasmids pMT183, pDK2, pMT414 and pMT413, respectively, using primer pair MipZ-uni2/MipZ-rev7. The PCR products were cut with *Nde*I and *Eco*RI and ligated into the *Nde*I/*Sac*I-treated target vector pBXMCS-2.

For the construction of pJR26, the parental plasmid pTB146 was cut with *Nde*I and *Xho*I and ligated with an *Nde*I/*Xho*I-treated PCR product containing the ***ftsZ*** gene, amplified with primer pair SUMO-for/ftsZ-rev-5 (*Nde*I/*Xho*I). To construct pJAK40, the backbone of *Nde*I/*Xho*I-treated pJR26 was fused by Gibson assembly with two DNA fragments that were obtained by PCR using primer pairs FtsZ-1-for/FtsZ-2-rev and FtsZ-3-for/FtsZ-4-rev, respectively, and plasmid pJR26 as a template. Plasmids pLC15 and pLC16 were generated by site-directed mutagenesis of pJR26 via inverse PCR with the mutagenic primer pairs FtsZ-N211A-for/-rev and FtsZ-D213A-for/-rev, respectively. Plasmid pLC58 was constructed analogously, using primer pair FtsZ-L277A-for/-rev, respectively. To construct plasmid pLC27, a DNA fragment amplified from pJR26 with the primer pair pET-For/FtsZ-3-rev was cut with *Nhe*I and *Bam*HI and ligated into *Nhe*I/*Bam*HI-treated pJR26. For the generation of plasmid pLC75, pJR26 was subjected to two rounds of site-directed mutagenesis by inverse PCR with the primer pairs ftsZ-F182E-for/-rev and ftsZ-L276E-for/-rev, respectively. To construct plasmid pLT1, pJR26 was treated with *Nde*I/*Xho*I and fused by Gibson assembly with a DNA fragment obtained by PCR using the primer pair ftsZ1-for-new/ftsZ-rev-6(182). To construct plasmid pLT2, pJR26 was treated with *Nde*I/*Xho*I and fused by Gibson assembly with two DNA fragments obtained by PCR using the primer pairs ftsZ1-for-new/ftsZ-rev-SUMO(183) and ftsZ-for-7(183)/ftsZ4-rev-new, respectively.

To construct *C. crescentus* strain LT2, plasmid pBH100 was integrated at the *vanA* (P*van*) locus (2) of strain EG384 (5) by single-homologous recombination. Subsequently, the native *mipZ* gene of the resulting strain was deleted by double-homologous recombination using plasmid pMT191 (6).

To generate *C. crescentus* strains LC33, LC34 and LC36 and JR65-JR69, plasmids pLC50, pLC51, or pBH78 or plasmids pJR107-pJR111, respectively, were integrated at the *xylX* (*Pxyl*) locus (1) of strain LT2 by single-homologous recombination.

Fluorescence microscopy

Cells were grown to exponential phase in vanillate-containing medium, washed and then cultivated for 6 h in medium containing 0.3% (w/v) xylose to deplete the native MipZ protein and induce the production of the different MipZ-eYFP variants. After immobilization on 1% (w/v) agarose pads, cells were imaged with a Zeiss Axio Observer.Z1 microscope (Zeiss, Germany) equipped with a Zeiss Plan-Apochromat 100x/1.40 Oil Ph3 M27 objective and a pco.edge sCMOS camera (PCO, Germany). An X-Cite 120PC metal halide light source (EXFO, Canada) and ET-YFP and ET-CFP filter cubes (Chroma, USA) were used for fluorescence detection. Images were recorded with VisiView (Visitron Systems, Germany) and analyzed with Fiji 1.49 (7). Minicells were defined as cells whose length was smaller than the minimum length of the wild-type strain.

Protein overproduction and purification

Rosetta(DE3)pLysS derivatives transformed with suitable plasmids were grown at 37 °C in LB medium. At an OD_{600} of 0.6-0.8, protein overproduction was induced by the addition of 1 mM IPTG. After three more hours of incubation (wild-type MipZ) or incubation at 25 °C overnight (F3 and D2 derivatives), the cells were harvested by centrifugation, washed with the corresponding resuspension buffer, snap-frozen in liquid nitrogen, and stored at -80 °C until further use.

To purify MipZ-His_6 and its mutant derivatives, cells were thawed and resuspended in 2 ml of buffer B3 (50 mM NaH_2PO_4, 300 mM NaCl, 20 mM imidazole, adjusted to pH 8 with NaOH) per gram of cell pellet, supplemented with 100 µg ml^{-1} PMSF (phenylmethylsulfonyl fluoride) and 10 µg ml^{-1} DNase I. After three passages through a French Press at 16,000 psi, cell debris was removed by centrifugation at 30,000 × g and 4 °C for 60 min. The supernatant was then passed through a 0.2 µm filter and loaded onto a 5 ml HisTrap HP Ni-NTA affinity column (GE Healthcare, USA). The column was washed with buffer B3, and protein was eluted with a linear gradient of imidazole (20-250 mM imidazole, 50 mM NaH_2PO_4, 300 mM NaCl, pH 8). Fractions containing the protein of interest were pooled and dialyzed at 4 °C in two steps against 3 l of buffer B6G (50 mM HEPES/NaOH pH 7.2, 50 mM NaCl, 5 mM $MgCl_2$, 0.1 mM EDTA, 10% (v/v) glycerol) (for HDX experiments) or buffer PG (50 mM HEPES/NaOH pH 7.2, 50 mM KCl, 5 mM $MgCl_2$, 10% (v/v) glycerol) (for all other experiments). After the removal of precipitates by centrifugation at 30,000 × g and 4 °C for 30 min, the protein was snap-frozen in liquid nitrogen and stored at -80 °C. Protein concentrations

were determined before every experiment with the Bradford assay, using the Roti-Nanoquant reagent (Carl Roth, Germany) with bovine serum albumin (Roth, Germany) as a standard.

Alternatively (for Fig. 5E and S7B-E), MipZ-His_6 and its mutant derivatives were first purified by Ni-NTA affinity chromatography as described above, using a linear gradient of imidazol (20-250 mM imidazole, 50 mM Tris/HCl, 300 mM KCl, 10% (v/v) glycerol, pH 8), and dialyzed against buffer B6G. Subsequently, the protein was loaded onto a 5 ml HiTrap SP HP cation exchange column (GE Healthcare, USA) and eluted with a linear gradient of NaCl (50-1000 mM NaCl, 100 mM HEPES/NaOH pH 7, 5 mM $MgCl_2$, 0.1 mM EDTA, 1 mM DTT). Fractions containing the protein of interest were pooled, dialyzed against buffer B7 (100 mM HEPES/NaOH pH 7, 50 mM NaCl, 5 mM $MgCl_2$, 0.1 mM EDTA, 1 mM DTT, 10% (v/v) glycerol), and then processed for storage as described above.

To purify native FtsZ or its mutant derivatives, cells overproducing the corresponding His_6-SUMO-FtsZ fusion proteins were resuspended in 2 ml of buffer BZ3 (50 mM Tris/HCl, 300 mM KCl, 250 mM imidazole, 10% (v/v) glycerol, pH 8) per gram of cell pellet, supplemented with DNase I (10 µg ml^{-1}), RNase I (2 µg ml^{-1}) and PMSF (100 µg ml^{-1}). After three passages through a French press at 16,000 psi, KCl was added to a final concentration of 1 M. The suspension was then centrifuged for 60 min at 30,000 × g. The supernatant was filtered through a membrane filter (0.22 µm pore size; Sarstedt, Germany) and loaded onto a 5 ml HisTrap HP or a 1 ml HisTrap FF Ni-NTA affinity column (GE Healthcare, Germany). After a wash of the columns with buffer BZK3 (buffer BZ3 with 1 M KCl), protein was eluted with buffer BZK4 (50 mM Tris/HCl, 1 M KCl, 250 mM imidazole, 10% (v/v) glycerol, pH 8). Fractions containing the protein of interest were pooled and dialyzed in two steps against 3 l of buffer B6G (for HDX experiments) or buffer PG (for all other experiments), both containing 20 ng $µl^{-1}$ DNase I and 20 ng $µl^{-1}$ RNase I. The His_6-SUMO tag was removed by incubation of the protein for 2 h at 4 °C with Ulp1-His_6 protease (0.5 µg per milligram of protein) in the presence of 1 mM DTT. His_6-SUMO and Ulp1-His_6 were then separated from FtsZ by Ni-NTA affinity chromatography on a 1 ml HisTrap FF column equilibrated with buffer B6G or buffer PG, respectively. Fractions of the flow-through containing pure FtsZ were pooled, aliquoted and stored at −80 °C until further use.

To purify StrepII-tagged FtsZ proteins (for Fig. 5E and S7C), His_6-SUMO-StrepII-FtsZ or its truncated variants were purified by Ni-NTA affinity chromatography as described above, with all buffers additionally containing 20 ng ml^{-1} DNaseI, 20 ng ml^{-1} RNaseI and 100 µg ml^{-1} PMSF. After dialysis of the protein against 3 l of buffer B6G containing 100 µg ml^{-1} PMSF, the His_6-SUMO tag was cleaved by treatment with Ulp1-His_6 protease. Subsequently, His_6-SUMO and Ulp1-His_6 were separated from FtsZ by Ni-NTA affinity chromatography on a 5 ml HisTrap FF column equilibrated with buffer B6G containing 100 µg ml^{-1} PMSF. After dialysis against the same buffer, the protein was further purified by size-exclusion chromatography on a HighLoad 16/60 Superdex 75 pg column (cytiva, USA) equilibrated with buffer B6G containing 100 µg ml^{-1} PMSF. Fractions containing pure protein were pooled, aliquoted and stored at −80 °C until further use.

Transmission electron microscopy

FtsZ (5 µM) was pre-incubated for 15 min at 25 °C in buffer P (50 mM HEPES/NaOH pH 7.2, 50 mM KCl, 5 mM $MgCl_2$) containing 1 mM ATPγS in the absence or presence of 7.5 µM MipZ. The reactions were then supplemented with 2 mM GTP (or 2 mM GMPPcP or 0.2 mM GMPcPP) and further incubated for 15 min. Alternatively, FtsZ was pre-incubated with GTP (or GMPcPP) in buffer P containing 1 mM ATPγS for 15 min, mixed with MipZ, and then incubated for another 15-60 min. For imaging, 5 µl aliquots of the samples were transferred to glow-discharged carbon-coated grids (G2400C; Plano Wetzlar, Germany). After 2 min of incubation, the grids were blotted with Whatman paper (Whatman, Germany), treated for 1 min with 2% (w/v) uranyl acetate, and then washed with water. Micrographs were taken with a JEM-2100 transmission electron microscope (JEOL, Japan) at an acceleration voltage of 120 kV. Images were captured with a 2k x 2k fast scan CCD camera F214 (TVIPS, Germany). Fiji 1.49 (7) was used for data analysis. The number of FtsZ monomers in a polymer was calculated using an average monomer diameter of 5 nm (8).

Bio-layer interferometry
Bio-layer interferometry analysis was performed with a BLItz System (Sartorius, USA) using Dip and Read High Precision Streptavidin Biosensors. For biotinylation, FtsZ was incubated with a 3-fold molar excess of EZ-Link NHS-PEG4-Biotin (Thermo Fisher Scientific, USA) for 1 h at 4 °C, followed by 15 min at room temperature. During the incubation, GTP was also present at 2 mM to reduce biotinylation at the polymerization interface. After the reaction, the protein was dialysed extensively against buffer PG to remove GTP and free NHS-PEG4-Biotin. All assays were performed at room temperature in buffer PG containing 0.01% (v/v) Triton X-100 and 0.01 mM BSA, with agitation at 2,200 rpm. FtsZ was immobilized on biosensors and probed with MipZ or its mutant variants (at the indicated concentrations), which had been pre-incubated in buffer PG for 5 min with 1 mM ATPγS. When indicated, a double-stranded DNA oligonucleotide (top strand: 5'-GCCGCCGC CGCCGCCGCCGC-3') was added at a concentration of 7.5 µM. The association step was followed by a washing step with buffer PG to dissociate MipZ from the immobilized FtsZ protein. To probe the interaction of MipZ with polymerized FtsZ, FtsZ was pre-incubated for 5, 10 or 60 min with 2 mM GMPPcP before immobilization. To determine the equilibrium dissociation constant (K_D), the maximal wavelength shifts measured at the end of the association phases were plotted against the corresponding protein concentrations. The data were then subjected to curve fitting using a one-site saturation ligand-binding model in SigmaPlot 14.5 (Systat Software, USA).

Nucleotide hydrolysis assays
GTPase and ATPase activities were measured using a continuous, regenerative coupled-enzyme assay (9). In brief, all assays (150 µl total volume) were performed at 25 °C in buffer P containing 20 U ml^{-1} pyruvate kinase (Sigma-Aldrich), 20 U ml^{-1} L-lactate dehydrogenase (Sigma-Aldrich), 600 µg ml^{-1} NADH and 3 mM phosphoenolpyruvate. GTPase reactions contained wild-type or mutant FtsZ (at the indicated concentration), 2 mM GTP and 1 mM ATPγS. When appropriate, 6 µM MipZ and/or 3 µM of a double-stranded DNA oligonucleotide (top strand: 5'-GCCGCCGCCGCCGCCGC CGC-3') were added. ATPase reactions contained 6 µM wild-type or mutant MipZ and 1 mM ATP. The linear decrease in the absorbance of NADH at 334 nm was monitored for 40 min in an Epoch 2 microplate reader (BioTek Instruments, USA). Activities were calculated using the molar extinction coefficient of NADH (6220 M^{-1} cm^{-1}) and an experimentally determined path length of 0.367 cm.

Sedimentation assays
FtsZ (3 µM) was pre-incubated for 15 min at room temperatur in buffer P containing 1 mM ATPγS in the absence or presence of 6 µM MipZ or its mutant derivatives. When indicated, a double-stranded DNA oligonucleotide (top strand: 5'-GCCGCCGCCGCCGCCGCCGC-3') was added at a concentration of 3 µM. The reactions were then supplemented with 2 mM GTP (or 2 mM GMPPcP or 0.2 mM GMPcPP) and further incubated for 15 min. Alternatively, FtsZ was pre-incubated with GTP (or GMPcPP) in buffer P containing 1 mM ATPγS for 15 min, mixed with MipZ, and then incubated for another 15-60 min. To sediment FtsZ polymers, the mixtures were centrifuged for 15 min at 385,900 × g and 25 °C using a Beckman MLA-130 rotor in a Beckman TL-100 ultracentrifuge (Beckman Coulter, USA). After immediate removal of the supernatants, the pellets were dissolved in 250 µL of SDS sample buffer and incubated for 5 min at 95 °C. Samples (10 µl) were loaded onto a 10% SDS-polyacrylamide gel, and proteins were visualized with Coomassie brilliant blue after electrophoresis. For the quantification of protein bands, gels were imaged with a ChemiDoc MP imaging system (Bio-Rad, USA) and analyzed using Image Lab 5.0 (Bio-Rad).

Fluorescence correlation spectroscopy (FCS)
All FCS measurements were performed in a self-made chamber as described previously (10). In brief, cover slides were rinsed thoroughly with acetone, ethanol and double-distilled water. 500 µl-plastic tubes (Eppendorf, Germany) were cut in halves and, after removal of the lid, glued to the cleaned cover slide with an ultraviolet (UV)-curing glue (Norland Adhesive 65; Norland Products, USA). The whole chamber was plasma-cleaned (MiniFlecto-PC-MFC, Germany) for 10 min at 0.3 mbar (DUO 5M vacuum pump; Pfeiffer Vacuum, Germany). The chambers were incubated with 100 µl of BSA (2 mg ml^{-1}) for approximately 20 min and washed 10 times with buffer P. Finally, all liquid was removed and 200 µl of buffer P were added immediately.

The confocal FCS experiments were performed on a LSM780 microscope equipped with a ConfoCor3 unit (Zeiss) in pseudo-crosscorrelation mode. All experiments were performed at a focal plane equal to 50 µm from the surface of the BSA-coated cover slide to avoid surface effects. The experimental autocorrelation curves typically showed at least two distinct decays, which we accounted for by fitting a model with two freely diffusing components of identical brightness *Q*1 = *Q*2. This special case of multicomponent diffusion is described by the autocorrelation function:

$$G_{3D+3D}(\tau) = (N_1 + N_2)^{-2} \sum_{j=1}^{2} \left[N_j \left(1 + \frac{\tau}{\tau_{D,j}}\right)^{-1} \left(1 + \frac{\tau}{S^2 \tau_{D,j}}\right)^{-1/2} \right]$$

where *f*1 = *N*1/(*N*1 + *N*2) and *f*2 = *N*2/(*N*1 + *N*2) represent the relative abundances of the two species. One of the two components is attributed to freely diffusing Alexa488 that is not attached to any protein. To minimize the number of free parameters, the diffusion coefficient of free Alexa488 was measured once accurately. After each daily calibration measurement, the diffusion time of Alexa488 was calculated for the measured detection volume size. This diffusion time was kept fixed for the first component for all fits.

To ensure that the FCS experiments were performed at irradiances that produced little to no photo-induced artifacts, a power series was acquired. The irradiance was estimated based on the power *P* after the objective, as measured with a power meter (PM100USB, Thorlabs, Germany) and a slide-mimicking detector (S170C, Thorlabs) that was directly positioned on the objective, including immersion fluid. The lateral beam diameter *wxy* was determined from the daily calibration measurements on freely diffusing fluorescent dye of known diffusion coefficient. Consequently, the peak irradiance in the focus reads $I_0 = 2P/(\pi\omega^2 xy)$. As expected, at low irradiances, the autocorrelation curves obtained decayed with the same lag times, whereas at high irradiances the triplet contribution becomes more pronounced and the autocorrelation curve shifts to shorter lag times. Moreover, the 3D+3D model does not hold any longer at large irradiances. Based on these findings, all experiments were performed at $I_0 = 2$ kW/cm^2.

The diffusion time of FtsZ was followed by a series of 2-min measurements for at least 40 min. The diffusion coefficient was calculated using $D = \omega^2_{xy}/4\tau_D$. The temperature at the objective ($T = 27$ °C) is assumed to be the sample temperature, which is expected to be accurate with a relative error below 1%. The viscosity of buffer P at this temperature was measured with a rolling ball viscosimeter together with a densiometer, and found to be $\eta = 0.878$ mPa s, which is only 3% higher than the viscosity of water.

Hydrogen-deuterium exchange mass spectrometry (HDX-MS)

7.5 µl of protein sample were mixed with D_2O-containing buffer B6 containing 1 mM ATPγS and/or 2 mM GMPPcP where applicable (see above) to a final volume of 75 µl. After incubation for 0.5, 1, 2 or 10 min at 25 °C, samples (55 µl) were taken from the reactions and mixed with an equal volume of quench buffer (400 mM KH_2PO_4/H_3PO_4, 2 M guanidine–HCl, pH 2.2), cooled to 1 °C. 95 µl of the mixture were immediately injected into an ACQUITY UPLC M-class system with HDX technology (Waters, USA) (11). Proteins were digested online with immobilized pepsin at 12 °C with a constant flow (100 µl min^{-1}) of water and 0.1% (v/v) formic acid, and the resulting peptic peptides were collected for 3 min on a C18 column (Waters) that was kept at 0.5 °C. The trap column was then placed in line with an ACQUITY UPLC BEH C18 1.7 µm 1.0 × 100 mm column (Waters), and the peptides were eluted at 0.5°C using a gradient of water + 0.1% (v/v) formic acid (eluent A) and acetonitrile + 0.1% (v/v) formic acid (eluent B) at a flow rate of 30 µl min^{-1} as follows: 0–7 min/95–65% A, 7–8 min/65–15% A, 8–10 min/15% A, 10–11 min/5% A, 11–16 min/95% A. Mass spectra of deuterated samples were acquired in High Definition MS positive ion mode using a G2-Si HDMS mass spectrometer equipped with an ESI source (Waters). Non-deuterated samples were prepared in the same way by incubation in non-deuterated buffer, with mass spectra recorded in Enhanced High Definition MS mode (12, 13). Continuous lock mass correction was performed using a [Glu1]-Fibrinopeptide B standard (Waters). All experiments were performed with three technical replicates. After each run, the pepsin column was washed three times with 80 µl of 4% (v/v) acetonitrile and 0.5 M guanidine–HCl. Additionally, blank runs were performed between each analysis to avoid

peptide carry-over. HDX-MS data analysis was performed as described previously (14). A full report of the data obtained is provided in Datasets S1-S4.

Supporting Figures

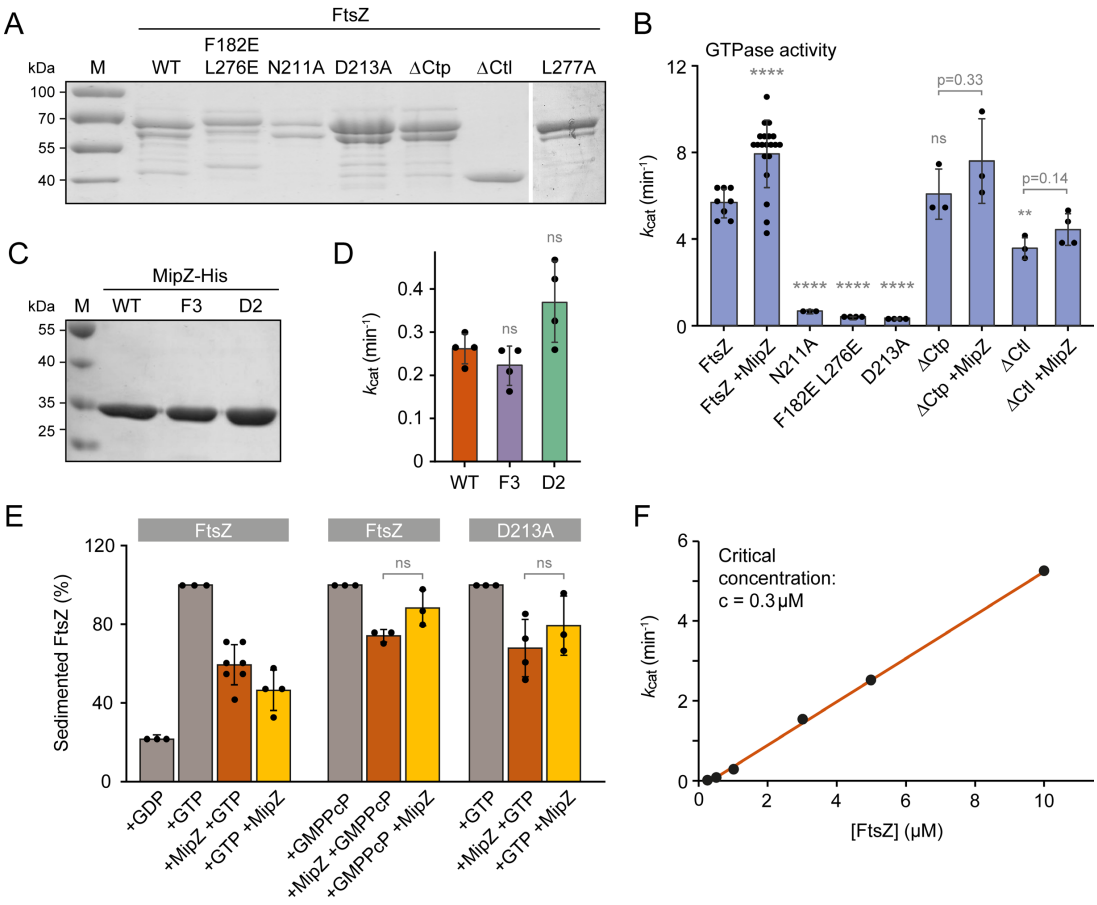

Fig. S1. Characterization of different FtsZ mutants. (**A**) Purity of the FtsZ preparations used in this study. Samples (15 µl) of the indicated proteins (5 µM) were analyzed by SDS-PAGE. Note that FtsZ (54.2 kDa) displays a higher apparent molecular weight in SDS gels (6), likely due to its high content of acidic amino acids. The bands of lower molecular weight represent degradation products of FtsZ, resulting from proteolytic cleavage in its non-structured C-terminal region. (**B**) GTPase activity of different FtsZ variants. The indicated proteins (2 µM) were assayed for GTPase activity in the presence or absence of MipZ•ATPγS (4 µM). The bar chart shows the average (± SD) of three to nineteen independent experiments (dots). The significance of differences to the result obtained for wild-type FtsZ in the absence of MipZ was assessed using the Student's t-test (ns: not significant, **** p<0.0001). (**C**) Purity of the MipZ variants used in this study. Samples (15 µL) of the indicated proteins (5 µM) were analyzed by SDS-PAGE. (**D**) ATPase activity of the indicated MipZ variants (6 µM) in the presence of 1 mM ATP. The bar chart shows the average (± SD) of four independent experiments (dots). The significance of differences to the wild-type protein was assessed using the Student's t-test (ns: not significant). (**E**) Sedimentation assay of $FtsZ_{wt}$ or $FtsZ_{D213A}$ in the presence of MipZ and GTP or GMPPcP. The indicated proteins (3 µM) were incubated with GTP or GMPPcP (2 mM) and, when indicated, with MipZ•ATPγS (6 µM) and subjected to ultracentrifugation. The bar chart shows the average percentage of pelleted FtsZ (± SD) from three to seven independent experiments (dots). Error bars indicate the standard deviation. Both full-length FtsZ and the most prominent proteolytic product (see Fig. S1A) were quantified. The significance of differences between reactions was assessed using the Student's t-test (ns: not significant). (**F**) Critical concentration of FtsZ. The GTPase activity of FtsZ was determined at different FtsZ concentrations. The critical concentration (minimal concentration required to observe activity) was estimated to be 0.3 µM.

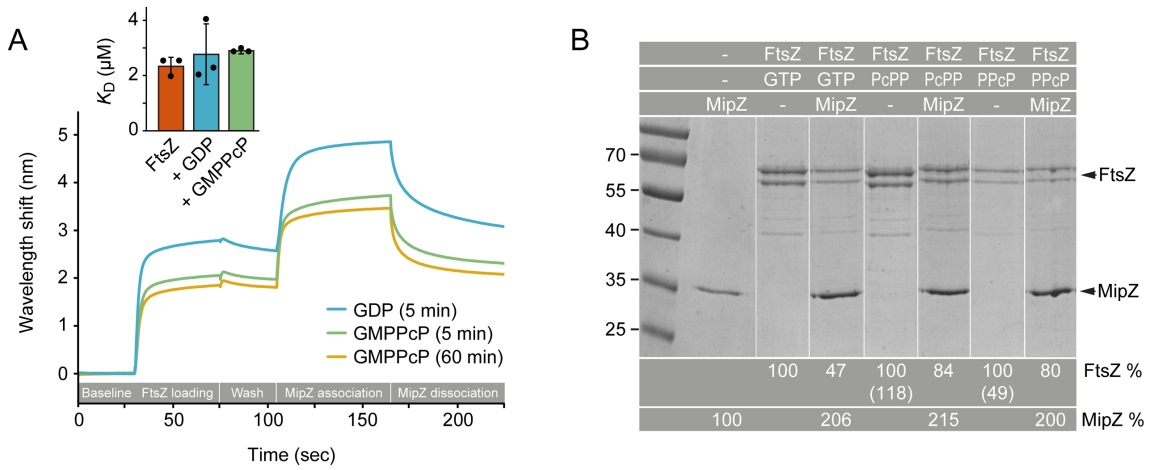

Fig. S2. MipZ is able to interact with polymeric FtsZ. (**A**) Bio-layer interferometry analysis of the interaction between FtsZ and MipZ. Biotinylated FtsZ was preincubated with 2 mM GDP or GMPPcP for the indicated times, immobilized on a streptavidin-coated biosensor and probed with MipZ•ATPγS (15 μM). The inset shows the affinities (K_D) of the interaction between MipZ•ATPγS and FtsZ under the indicated conditions. The values were calculated based on the observed association and dissociation rates. Data represent the average (± SD) of three independent experiments. (**B**) Effect of MipZ on the sedimentation of FtsZ. Reactions containing the indicated components were incubated for 15 min and subjected to ultracentrifugation. Shown is a representative SDS-gel loaded with the pellet fractions. For each nucleotide, the amount of FtsZ sedimented in reactions without MipZ was set to 100% and compared to the amount sedimented with MipZ. The values in brackets give the relative amounts of FtsZ sedimented in reactions with GMPcPP or GMPPcP in comparison to the reaction with GTP.

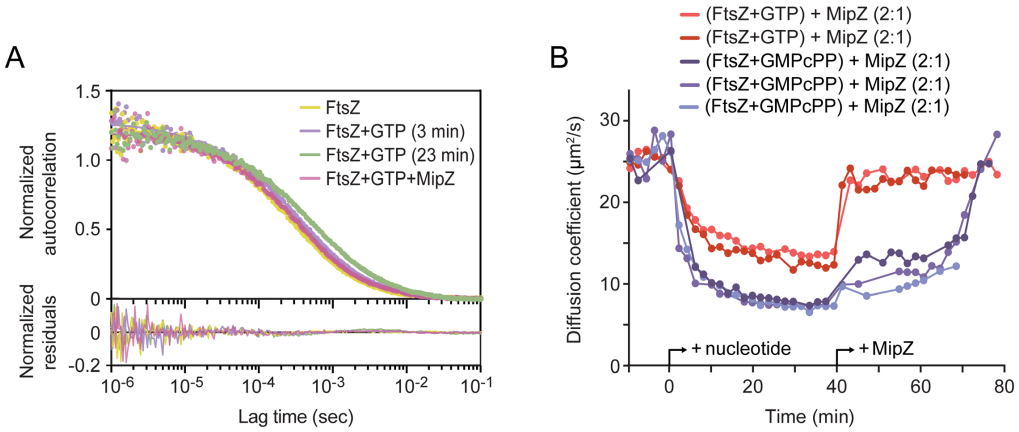

Fig. S3. FtsZ polymerization dynamics observed by fluorescence correlation spectroscopy (FCS). (**A**) Representative normalized autocorrelation curves of FtsZ (2 μM), recorded at different times after the addition of GTP (2 mM) and MipZ•ATPγS (1 μM) and overlaid with the corresponding fit (see Methods). The bottom panel shows the residuals of the fitted curves. (**B**) Time evolution of the diffusion coefficient of FtsZ. FtsZ (2 μM), containing 10% AlexaFluor488-labeled protein, was analyzed by FCS at 2 min intervals prior to and after the addition of the indicated nucleotide (2 mM for GTP, 0.2 mM for GMPcPP) and MipZ•ATPγS (1 μM), generated by preincubation of MipZ with 1 mM ATPγS.

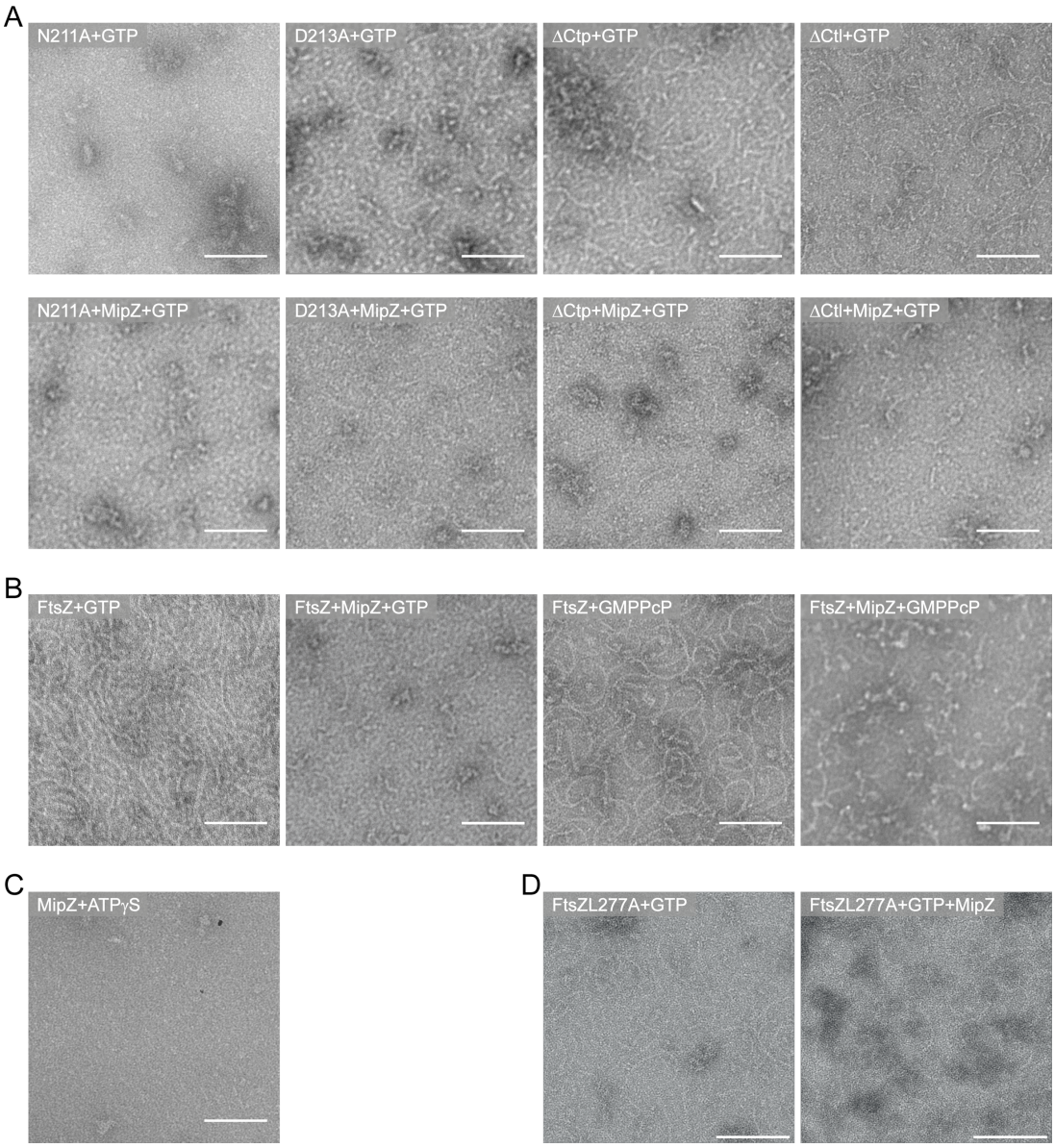

Fig. S4. FtsZ polymerization observed by transmission electron microscopy. (**A**) Transmission electron microscopy (TEM) images of different FtsZ variants. The indicated FtsZ derivatives were incubated with nucleotides (2 mM) in the absence or presence of MipZ•ATPγS (7.5 μM), stained with uranyl acetate and visualized by TEM. Scale bars: 100 nm. (**B**) TEM images of native FtsZ incubated with nucleotides (2 mM) in the absence or presence of MipZ•ATPγS (7.5 μM). Scale bars: 100 nm. (**C**) TEM image of MipZ (7.5 μM) incubated with ATPγS (1 mM). Scale bar: 100 nm. (**D**) TEM images of $FtsZ_{L277A}$ incubated with GTP (2 mM) in the absence or presence of MipZ•ATPγS (7.5 μM). Scale bars: 100 nm.

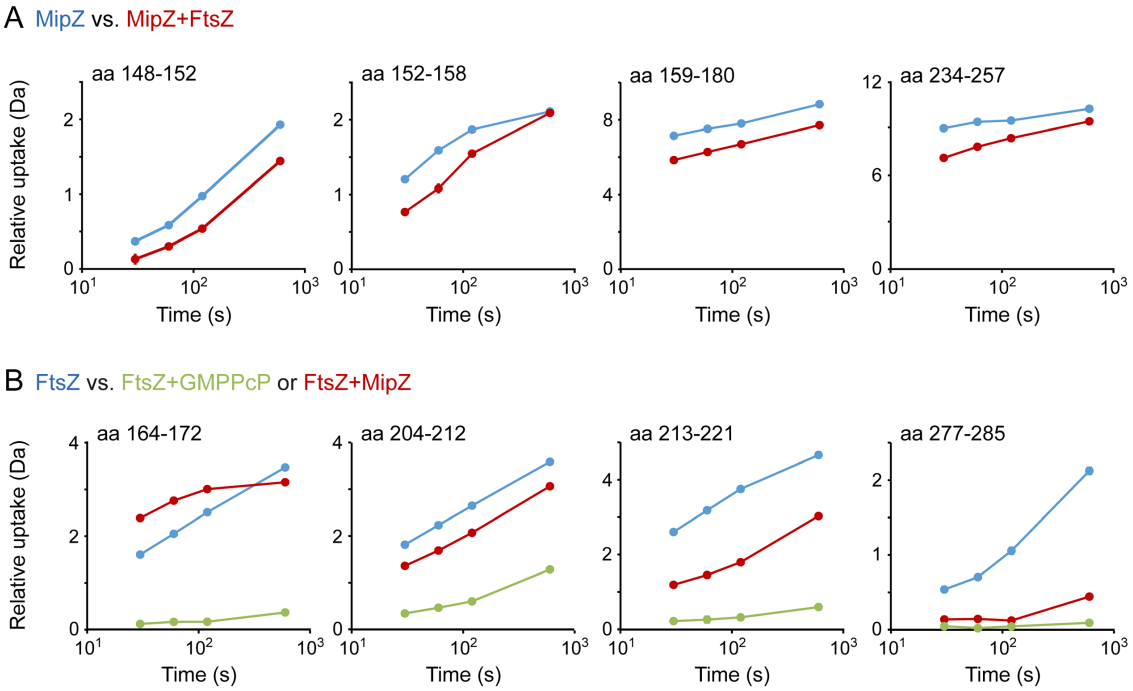

Fig. S5. HDX rates of representative peptides from MipZ and FtsZ. (**A**) The graphs show the average (± SD) deuterium uptake of representative peptides from MipZ obtained in the absence (blue) or presence (red) of FtsZ from one representative experiment. (**B**) The graphs show the average (± SD) deuterium uptake of representative peptides obtained for FtsZ alone (blue), in the presence of GMPPcP (green) or in the presence of MipZ (red) from one representative experiment.

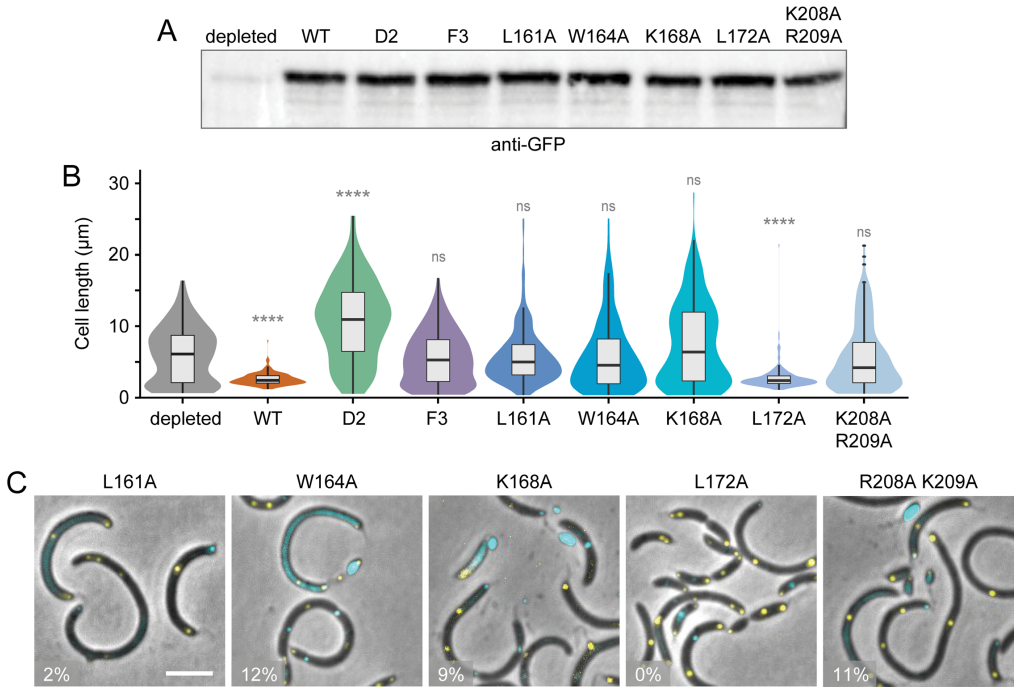

Fig. S6. ***In vivo*** **functionality of MipZ variants with substitutions in the FtsZ-specific site.** (**A**) Immunoblot analysis of *C. crescentus* cells producing the indicated MipZ-eYFP variants in place of the wild-type protein. Strains LC36 (WT), LC34 (D2), LC33 (F3), JR65 (L161A), JR66 (W164A), JR67 (K168A), JR68 (L172A) and JR69 (K208A R209A) were grown to exponential phase in vanillate-containing medium, washed and then cultivated for 6 h in medium containing 0.3% (w/v) xylose to deplete the native MipZ protein and induce the production of the indicated fusion proteins. As a control, cells of LC36 were also analyzed without induction of the complementing wild-type MipZ-eYFP fusion (depleted). Samples of the cultures were subjected to immunoblot analysis with an anti-GFP antibody. (**B**) Distribution of cell lengths in the cultures described in (A). The data are shown as box plots, as defined in Fig. 3C**.** In addition, rotated kernel density plots are given for each dataset to indicate the distribution of the data. (**C**) Subcellular localization and functionality of different MipZ-eYFP variants. Shown are overlays of phase contrast and fluorescence images of MipZ-depleted cells producing the indicated MipZ-eYFP variants as well as mCherry-FzlA (false-colored in cyan) as a proxy for the divisome. The cultures were grown as described in (A). The percentage of minicells produced by each strain is given in the lower left corner of the images (n=200 cells per strain). Scale bar: 3 µm.

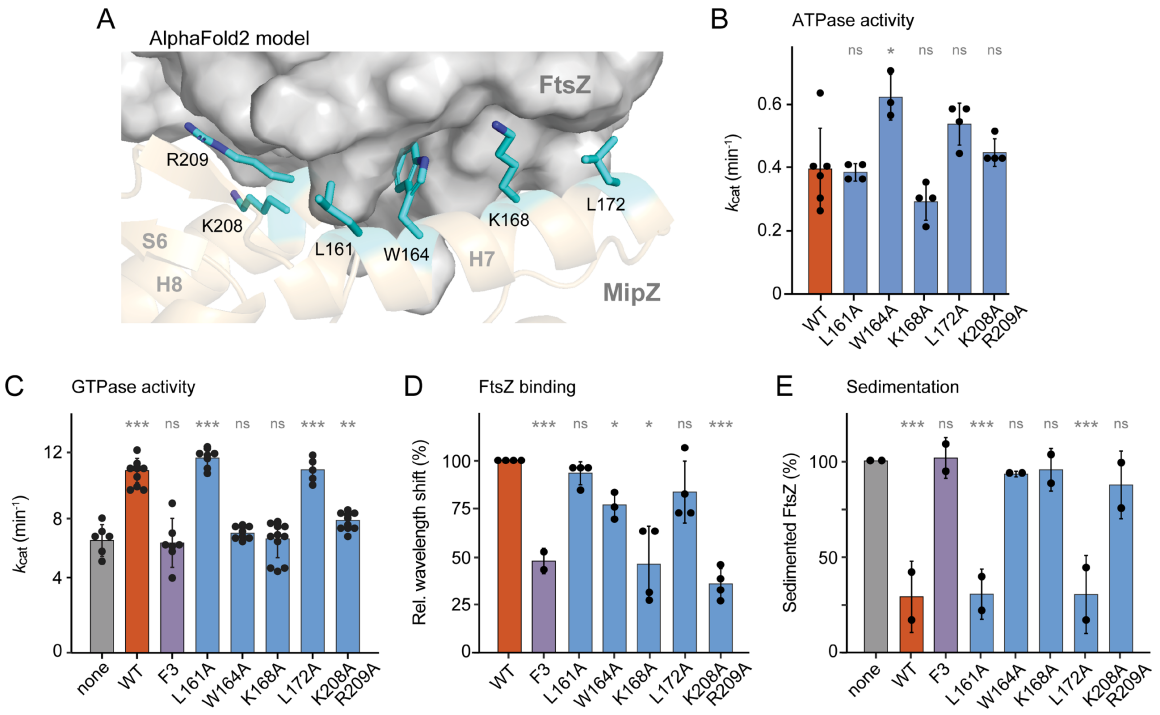

Fig. S7. Biochemical activities of MipZ variants with substitutions in the FtsZ-specific site. (**A**) Model of the MipZ-FtsZ interface generated with AlphaFold-Multimer (15). The CTD of FtsZ is shown in surface view. Exposed charged and hydrophobic residues in the FtsZ-specific site of MipZ are shown in cyan. Oxygen and nitrogen atoms are highlighted in red and blue, respectively. Secondary structural elements of MipZ located in the interface region are shown in cartoon view. See **Fig. S8** for details. (**B**) ATPase activities of the indicated MipZ variants (6 μM) in the presence of 1 mM ATP. The bar chart shows the average (± SD) of three to six independent experiments (dots). (**C**) GTPase activity of FtsZ in the presence of different MipZ variants. FtsZ (3 μM) was incubated with 2 mM GTP in absence (none) or presence of the indicated MipZ•ATPγS variants (6 μM). The bar chart shows the average (± SD) of five to eleven independent experiments (dots). (**D**) Bio-layer interferometry analysis of the interaction between FtsZ and the indicated MipZ variants, performed as in Fig. 1B. Shown are the average relative wavelength shifts (± SD) measured after equilibration of the binding reactions, normalized to the value obtained for the interaction of FtsZ with wild-type MipZ. (**E**) Effects of different MipZ variants on FtsZ polymerization. FtsZ (3 μM) was incubated with 2 mM GTP in the absence (none) or presence of the indicated MipZ•ATPγS variants (6 μM) and subjected to ultracentrifugation. The bar chart shows the average (± SD) amount of sedimented FtsZ recovered from the pellet. Data represent the results of four independent experiments (dots). In panels B-E, the statistical significance of differences between the first and the remaining conditions shown in the graphs was assessed using the Student's t-test (ns: not significant, * p<0.05, ** p<0.001, *** p<0.0001).

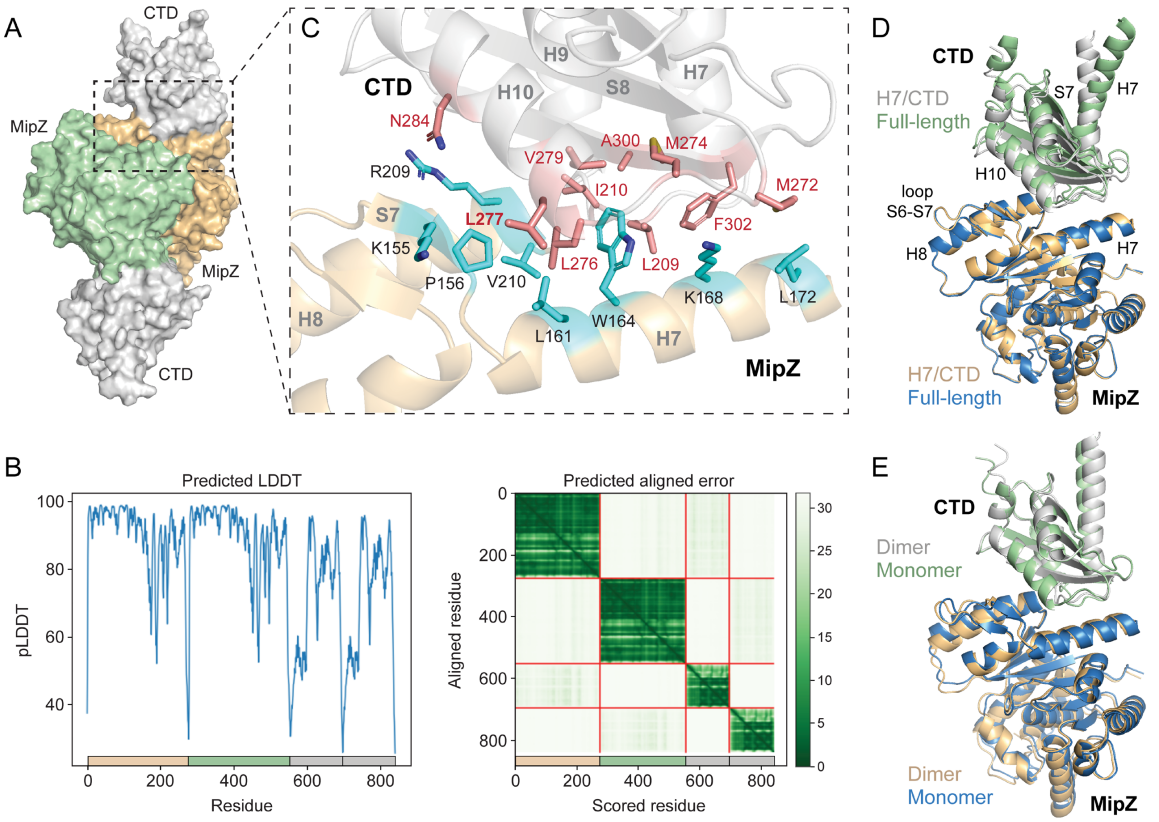

Fig. S8. Model of the MipZ-FtsZ complex. (**A**) Surface view of the MipZ dimer-FtsZ complex. The structure of the complex was predicted with AlphaFold-Multimer (15), using the sequences of two MipZ molecules and two FtsZ fragments (amino acids 183-320) comprising only helix H7 and the CTD as a starting point. Note that the predicted structure of the MipZ dimer is highly similar to the published crystal structure of the MipZ dimer (PDB: 2XJ9) (16), with a root-mean-square deviation (rmsd) of 0.505 Å over 452 paired Cα atoms. Likewise, the model of the FtsZ fragment shows high similarity to the corresponding region in the crystal structure of FtsZ•GTPγS from *Staphylococcus aureus* (PDB: 3WGN) (17), with an rmsd of 2.228 Å over 125 paired Cα atoms. (**B**) Confidence measures for the predicted MipZ $FtsZ_{H7/CTD}$ complex. The plots show the predicted local distance difference test (pLDDT) and the predicted aligned error for the MipZ-$FtsZ_{T7/CTD}$ complex shown in panel A provided by AlphaFold-Multimer. (**C**) Architecture of the MipZ-FtsZ interface in the predicted dimeric MipZ-$FtsZ_{T7/CTD}$ complex. The fold of the two proteins in the interface region is visualized in cartoon view. Relevant residues are shown in stick view and colored cyan (MipZ) and red (FtsZ), respectively. Nitrogen atoms are indicated in blue, oxygen atoms in red. For clarity, backbone atoms are not displayed. (**D**) Comparison of the predicted MipZ-$FtsZ_{T7/CTD}$ complex from panel A with a MipZ-full-length FtsZ complex, predicted by AlphaFold-Multimer using the sequences of two MipZ molecules and one FtsZ molecule. For clarity, only one MipZ molecule and only the region corresponding to $FtsZ_{T7/CTD}$ are shown. (**E**) Comparison of the predicted MipZ-$FtsZ_{T7/CTD}$ complex from panel A with that of a MipZ monomer-$FtsZ_{T7/CTD}$ complex. For clarity, only a subcomplex of the dimeric structure is shown.

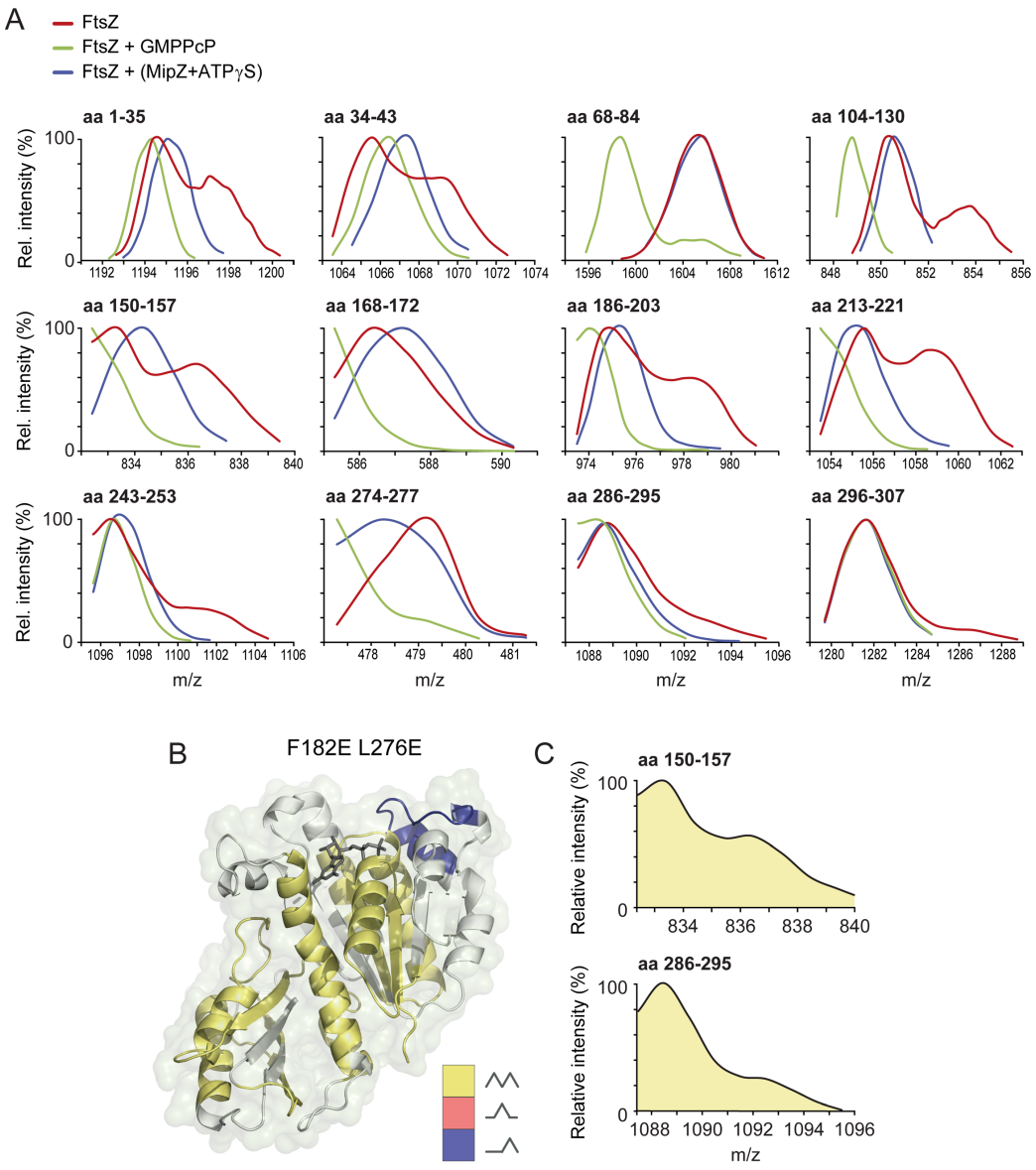

Fig. S9. Conformational dynamics of FtsZ under different conditions. (**A**) Modality of the mass/charge ratios of representative peptides from wild-type FtsZ. The graphs show the distributions of the mass/charge ratios of representative peptides of FtsZ obtained after HDX analysis alone or in the presence of GMPPcP (2 mM) or MipZ•ATPγS after 60 s of deuteration. (**B**) Modality of the distributions of the peptide mass/charge ratios obtained by HDX analysis of $FtsZ_{F182E/L276E}$, plotted onto a structural model of *C. crescentus* FtsZ. (**C**) Distribution of the mass/charge ratios for two representative peptides from $FtsZ_{F182E/L276E}$ (amino acids 150-157 and amino acids 286-295) after 60 s of deuteration.

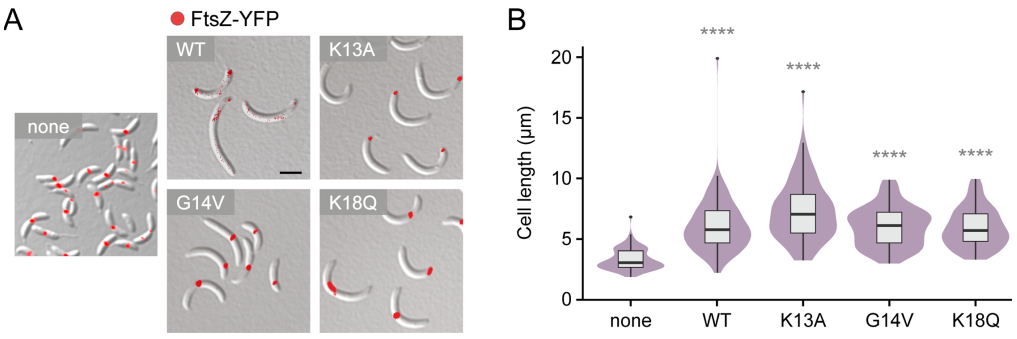

Fig. S10. *In vivo* analysis of the interaction between MipZ and FtsZ. (**A**) Phenotype and FtsZ localization pattern of cells overproducing different MipZ variants. Strain MT199 (P*van-ftsZ-eyfp)* (none) or derivatives of MT199 carrying xylose-inducible alleles of wild-type MipZ (TR19) or its monomeric K13A (TR16), K18Q (TR17) or G14V (TR18) variants on medium-copy-number plasmids were grown in PYE medium and induced with xylose and vanillate for 3 h to induce the production of FtsZ-YFP and the indicated MipZ variants. Shown are overlays of differential interference contrast and fluorescence images. (**B**) Box plots, as defined in Fig. 3C, and rotated kernel density plots showing the distribution of cell lengths in the cultures analyzed in (A). The statistical significance of differences to the background strain MT199 was tested using the Student's t-test (**** p<0.0001).

Supporting Tables

Table S1. Oligonucleotides used in this work.

Name	Sequence (5' to 3') [1)]
pET-For	cacgatgcgtccggcgtagaggatc
FtsZ-1-for	atatGCTCTTCGGGTatggctatttctctttccgcgccg
FtsZ-2-rev	atcggctgcagttgcgggttgcgcgacacgggct
FtsZ-3-for	agcccgtgtcgcgcaacccgcaactgcagccgat
FtsZ-3-rev	cctcggGGATCCctaggcctgcggcgtttc
FtsZ-4-rev	atatGGATCCtcagttggccaggcggcgcag
ftsZ1-for-new	tggttctcaccaccaccaccaccatatggctagccgatcggact
ftsZ-rev-6(182)	agtcacccgggctcgactagaaggtcgtgcgctcg
ftsZ-rev-SUMO(183)	catgccgaaggcttcggcaccaccaatctgttctctg
ftsZ-for-7(183)	cagagaacagattggtggtgccgaagccttcggcatg
ftsZ4-rev-new	tcacccgggctcgagtcagttggccagg
ftsZ-rev-5	tataCTCGAGtcagttggccaggcggcgcaggaac
FtsZ-F182E-for	aacgagcgcacgaccgaggccgaagccttcggc
FtsZ-F182E-rev	gccgaaggcttcggcctcggtcgtgcgctcgtt
FtsZ-N211A-for	gccgggcctgatcgccctcgacttcgcc
FtsZ-N211A-rev	ggcgaagtcgagggcgatcaggcccggc
FtsZ-D213A-for	cctgatcaacctcgccttcgccgacgtcc
FtsZ-D213A-rev	ggacgtcggcgaaggcgaggttgatcagg
FtsZ-R218A-for	cttcgccgacgtcgccacggtcatgaccgag
FtsZ-R218A-rev	ggtcatgaccgtggcgacgtcggcgaagtcgag
FtsZ-L277A-for	catggacatgaccttggcggaagtcgacgaggcc
FtsZ-L277A-rev	ggcctcgtcgacttccgccaaggtcatgtccatg
FtsZC_NdeI	attaCATATGgccgaagccttcggcatggccgacc
FtsZ_full_SacI	atGAGCTCagttggccaggcggcgcaggaacg
Gibson_Strep_ftsZ_for	cgaaaaaggttcgggctctcatatggctatttctctttccgcgccgcg
Gibson_ftsZ_rev	gccgcaagcttgtcgacggagctcagttggccaggcggcgcaggaacg
Gibson_Strep-ftsZ-dCDR_rev	gccgcaagcttgtcgacggagctcagtccatgccggtggcgacgaccgac
MipZ-Gib-for	ggagacgacCATATGgccgaaacgcgcgttatcg
MipZ-Gib-rev	gaattctccgGAGCTCgcgccgccagcatcgtc
MipZ-uni2	TTTCATatggccgaaacgcgcgttatcgtcg
MipZ-rev10	TTGAGCTCgcgccgccagcatcgtctcgccgga
MipZ-rev-EcoRI	ttGAATTCttactgcgccgccagcatcgtctc
MipZ-rev7	tatGAGCTCcctgcgccgccagcatcgtctcgcc
MipZ-K155A-for	accctggagctgaccgcgcccagcctctattc
MipZ-K155A-rev	gaatagaggctgggcgcggtcagctccagggt
MipZ-W164A-for	tgggaaggtcgcgcgcagcgcgccc
MipZ-W164A-rev	gggcgcgctgcgcgcgaccttccca
MipZ-R167AK168A-for	cgctgaccgtctgggaaggtgccgcgcagcgcgccctgtcg
MipZ-R167AK168A-rev	gggcgcgctgcgcggcaccttcccagacggtcagcg
MipZ-R194A-for	caccaccgaggcggcgaaccgcaagcgt
MipZ-R194A-rev	acgcttgcggttcgccgcctcggtggtg
MipZ-K208AR209A-for	cctcaacgctttggccgcggccgtcggcttccggatc
MipZ-K208AR209A-rev	gatccggaagccgacggccgcggccaaagcgttgagg
MipZ-R219A-for	ggcccggcctggccgaccgcgtga
MipZ-R219A-rev	tcacgcggtcggccaggccgggcc
SUMO-for	tataCATATGgctagcggatcggactcagaag

[1)] Restriction sites are indicated by capital letters.

Table S2. Plasmids used in this work.

Plasmid	Description [1)]	Reference
pBH78	pXYFPC-2 carrying *mipZ$_{WT}$*	(18)
pBXMCS-2	Replicating plasmid for the overexpression of genes under the control of *Pxyl*, Km^R	(2)
pDK2	pET21a(+) carrying *his-mipZK13A*	(16)
pMT183	pET21a(+) carrying *his-mipZ*	(6)
pMT191	Plasmid for the construction of an in-frame deletion in *mipZ*	(6)
pMT413	pET21a(+) carrying *his-mipZG14V*	(6)
pMT414	pET21a(+) carrying *his-mipZK18Q*	(6)
pTB146	ColE1 *bla lacI^q* P$_{T7}$::*his-sumo*, Ap^R	(19)
pVCERN-1	Plasmid for the integration of a gene fused to the 3'-end of *venus* at the *vanA* (*Pvan*) locus of *C. crescentus*, Sp^R	(2)
pXYFPC-2	Plasmid for integration of a gene fused to 5'-end of *eyfp* at the *xylX* (*Pxyl*) locus of *C. crescentus*, Km^R	(2)
pBH100	pVCERN-1 carrying *mipZ$_{WT}$*	This study
pJAK40	pTB146 carrying *his-sumo-ftsZdCtI (FtsZΔ336-480)*, Ap^R	This study
pJR26	pTB146 carrying *his-sumo-ftsZ,* Ap^R	This study
pJR99	pTB146 carring *his-sumo-strepII,* Ap^R	
pJR100	pET21a(+) carrying *his-mipZL161A*, Ap^R	This study
pJR101	pET21a(+) carrying *his-mipZW164A*, Ap^R	This study
pJR102	pET21a(+) carrying *his-mipZK168A*, Ap^R	This study
pJR103	pET21a(+) carrying *his-mipZL172A*, Ap^R	This study
pJR104	pTB146 carrying *his-sumo-strepII-ftsZ,* Ap^R	This study
pJR105	pTB146 carrying *his-sumo-strepII-ftsZΔN,* Ap^R	This study
pJR106	pTB146 carrying *his-sumo-strepII-ftsZΔNC,* Ap^R	This study
pJR107	pXYFPC-2 carrying *mipZL161A*, Km^R	This study
pJR108	pXYFPC-2 carrying *mipZW164A*, Km^R	This study
pJR109	pXYFPC-2 carrying *mipZK168A*, Km^R	This study
pJR110	pXYFPC-2 carrying *mipZL172A*, Km^R	This study
pJR111	pXYFPC-2 carrying *mipZK208AR209A*, Km^R	This study
pLC15	pTB146 carrying *his-sumo-ftsZN211A*, Ap^R	This study
pLC16	pTB146 carrying *his-sumo-ftsZD213A*, Ap^R	This study
pLC27	pTB146 carrying *his-sumo-ftsZdCtp (FtsZ 1-491)*, Ap^R	This study
pLC45	pET21a(+) carrying *his-mipZF3* (K155A R167A K168A), Ap^R	This study
pLC46	pET21a(+) carrying *his-mipZD2* (R194A R219A), Ap^R	This study
pLC50	pXYFPC-2 carrying *mipZF3* (K155A R167A K168A), Km^R	This study
pLC51	pXYFPC-2 carrying *mipZD2* (R194A R219A), Km^R	This study
pLC58	pTB146 carrying *his-sumo-ftsZL277A*, Ap^R	This study
pLC75	pTB146 carrying *his-sumo-ftsZF182EL276E,* Ap^R	This study
pLT1	pTB146 carrying *his-sumo-ftsZ(1-182)*, Ap^R	This study
pLT2	pTB146 carrying *his-sumo-ftsZ(183-508)*, Ap^R	This study
pLT7	pTB146 carrying *his-sumo-ftsZR167AK168A*, Ap^R	
pLT11	pET21a(+) carrying *his-mipZK208AR209A*, Ap^R	This study
pTR11	pBXMCS-2 carrying *mipZ*, Km^R	This study
pTR32	pBXMCS-2 carrying *mipZ$_{K13A}$*, Km^R	This study
pTR33	pBXMCS-2 carrying *mipZ$_{K18Q}$*, Km^R	This study
pTR34	pBXMCS-2 carrying *mipZ$_{G14V}$*, Km^R	This study

[1)] Ap^R: ampicillin resistance; Km^R: kanamycin resistance

Table S3. Strains used in this work.

Strains	Description/ genotype	Reference
CB15N	Wild-type strain of *C. crescentus*	(20)
EG384	CB15N *fzlA::mCherry-fzlA*	(5)
MT199	CB15N *Pvan::Pvan-ftsZ-yfp Pxyl::Pxyl-mipZwt*	(6)
Rosetta2(DE3)pLysS	*E. coli* strain for protein overproduction	Novagen
TOP10	*E. coli* strain for general cloning purposes	Invitrogen
JR65	CB15N *fzlA::mCherry-fzlA* Δ*mipZ Pvan::Pvan-mipZ Pxyl::Pxyl-mipZL161A*	This study
JR66	CB15N *fzlA::mCherry-fzlA* Δ*mipZ Pvan::Pvan-mipZ Pxyl::Pxyl-mipZW164A*	This study
JR67	CB15N *fzlA::mCherry-fzlA* Δ*mipZ Pvan::Pvan-mipZ Pxyl::Pxyl-mipZK168A*	This study
JR68	CB15N *fzlA::mCherry-fzlA* Δ*mipZ Pvan::Pvan-mipZ Pxyl::Pxyl-mipZL172A*	This study
JR69	CB15N *fzlA::mCherry-fzlA* Δ*mipZ Pvan::Pvan-mipZ Pxyl::Pxyl-mipZK208AR209A*	This study
LT2	CB15N *fzlA::mCherry-fzlA* Δ*mipZ Pvan::Pvan-mipZ*	This study
LC33	CB15N *fzlA::mCherry-fzlA* Δ*mipZ Pvan::Pvan-mipZ Pxyl::Pxyl-mipZF3* (K155A R167A K168A)	This study
LC34	CB15N *fzlA::mCherry-fzlA* Δ*mipZ Pvan::Pvan-mipZ Pxyl::Pxyl-mipZD2* (R194A R219A)	This study
LC36	CB15N *fzlA::mCherry-fzlA* Δ*mipZ Pvan::Pvan-mipZ Pxyl::Pxyl-mipZwt*	This study
TR16	CB15N *Pvan::Pvan-ftsZ-yfp* pTR32 (*Pxyl-mipZ*$_{K13A}$)	This study
TR17	CB15N *Pvan::Pvan-ftsZ-yfp* pTR33 (*Pxyl-mipZ*$_{K18Q}$)	This study
TR18	CB15N *Pvan::Pvan-ftsZ-yfp* pTR34 (*Pxyl-mipZ*$_{G14V}$)	This study
TR19	CB15N *Pvan::Pvan-ftsZ-yfp* pTR11 (*Pxyl-mipZ*)	This study

Legends to Supplemental Datasets

Dataset S1 (separate file). HDX profiles of MipZ$_{D42A}$•ATPγS in the absence and presence of FtsZ. The file contains (**A**) a summary of the conditions used for the HDX analysis, (**B**) a list of the peptides obtained in the different experiments and (**C**) a primary analysis of the data.

Dataset S2 (separate file). HDX profiles of FtsZ in the absence and presence of MipZ$_{D42A}$ or GMPPcP. The file contains (**A**) a summary of the conditions used for the HDX analysis, (**B**) a list of the peptides obtained in the different experiments and (**C**) a primary analysis of the data.

Dataset S3 (separate file). Comparison of the HDX profiles MipZ$_{D42A}$•ATPγS in the absence and presence of FtsZ, FtsZ$_{\Delta NC}$ or FtsZ$_{\Delta N}$. The file contains (**A**) a summary of the conditions used for the HDX analysis, (**B**) a list of the peptides obtained in the different experiments and (**C**) a primary analysis of the data.

Dataset S4 (separate file). Comparison of the HDX profiles of FtsZ and FtsZ$_{F182E/L276E}$ monomers. The file contains (**A**) a summary of the conditions used for the HDX analysis, (**B**) a list of the peptides obtained in the different experiments and (**C**) a primary analysis of the data.

SI References

1. A. C. Meisenzahl, L. Shapiro, U. Jenal, Isolation and characterization of a xylose-dependent promoter from *Caulobacter crescentus*. *J. Bacteriol.* 179, 592-600 (1997).
2. M. Thanbichler, A. A. Iniesta, L. Shapiro, A comprehensive set of plasmids for vanillate- and xylose-inducible gene expression in *Caulobacter crescentus*. *Nucleic Acids Res.* 35, e137 (2007).
3. D. G. Gibson *et al.*, Enzymatic assembly of DNA molecules up to several hundred kilobases. *Nat. Methods* 6, 343-345 (2009).
4. J. G. Marblestone *et al.*, Comparison of SUMO fusion technology with traditional gene fusion systems: enhanced expression and solubility with SUMO. *Protein Sci.* 15, 182-189 (2006).
5. E. D. Goley, N. A. Dye, J. N. Werner, Z. Gitai, L. Shapiro, Imaging-based identification of a critical regulator of FtsZ protofilament curvature in *Caulobacter*. *Mol. Cell* 39, 975-987 (2010).
6. M. Thanbichler, L. Shapiro, MipZ, a spatial regulator coordinating chromosome segregation with cell division in *Caulobacter*. *Cell* 126, 147-162 (2006).
7. J. Schindelin *et al.*, Fiji: an open-source platform for biological-image analysis. *Nat. Methods* 9, 676-682 (2012).
8. S. Hou *et al.*, Characterization of *Caulobacter crescentus* FtsZ protein using dynamic light scattering. *J. Biol. Chem.* 287, 23878–23886 (2012).
9. E. Ingerman, J. Nunnari, A continuous, regenerative coupled GTPase assay for dynamin-related proteins. *Methods Enzymol.* 404, 611-619 (2005).
10. B. Ramm, P. Glock, P. Schwille, *In vitro* reconstitution of self-organizing protein patterns on supported lipid bilayers. *J. Vis. Exp.* 137, e58139 (2018).
11. T. E. Wales, K. E. Fadgen, G. C. Gerhardt, J. R. Engen, High-speed and high-resolution UPLC separation at zero degrees Celsius. *Anal. Chem.* 80, 6815-6820 (2008).
12. S. J. Geromanos *et al.*, The detection, correlation, and comparison of peptide precursor and product ions from data independent LC-MS with data dependant LC-MS/MS. *Proteomics* 9, 1683-1695 (2009).
13. G. Z. Li *et al.*, Database searching and accounting of multiplexed precursor and product ion spectra from the data independent analysis of simple and complex peptide mixtures. *Proteomics* 9, 1696-1719 (2009).
14. M. Osorio-Valeriano *et al.*, ParB-type DNA segregation proteins are CTP-dependent molecular switches. *Cell* 179, 1512-1524 (2019).
15. R. Evans *et al.* (2022) Protein complex prediction with AlphaFold-Multimer. *bioRxiv* [preprint], DOI: 10.1101/2021.10.04.463034.
16. D. Kiekebusch, K. A. Michie, L. O. Essen, J. Löwe, M. Thanbichler, Localized dimerization and nucleoid binding drive gradient formation by the bacterial cell division inhibitor MipZ. *Mol. Cell* 46, 245-259 (2012).
17. T. Matsui, X. Han, J. Yu, M. Yao, I. Tanaka, Structural change in FtsZ induced by intermolecular interactions between bound GTP and the T7 loop. *J. Biol. Chem.* 289, 3501-3509 (2014).
18. L. Corrales-Guerrero *et al.*, Molecular architecture of the DNA-binding sites of the P-loop ATPases MipZ and ParA from *Caulobacter crescentus*. *Nucleic Acids Res.* 48, 4769-4779 (2020).
19. F. O. Bendezu, C. A. Hale, T. G. Bernhardt, P. A. de Boer, RodZ (YfgA) is required for proper assembly of the MreB actin cytoskeleton and cell shape in *E. coli*. *EMBO J.* 28, 193-204 (2009).
20. M. Evinger, N. Agabian, Envelope-associated nucleoid from *Caulobacter crescentus* stalked and swarmer cells *J. Bacteriol.* 132, 294-301 (1977).